Marine Gravity Anomaly from Satellite Altimetry: a Comparison of Methods over Shallow Waters

Cheinway Hwang, Hsin-Ying Hsu
Department of Civil Engineering, National Chiao Tung University, Taiwan.
hwang@geodesy.cv.nctu.edu.tw

Xiaoli Deng
Department of Spatial Sciences, Curtin University of Technology, Perth, Australia.

Abstract. Gravity anomalies over shallow waters are useful in many geodetic and geophysical applications. This work compares three methods of gravity anomaly derivation from altimetry over shallow waters near Taiwan: (1) compute gravity anomalies by LSC using along-track, differenced geoidal heights and height slopes, (2) compute gravity anomalies by least-squares collocation (LSC) using altimeter-derived along-track deflections of vertical (DOV), and (3) grid along-track deflections of vertical by LSC and then compute gravity anomalies by the inverse Vening Meinesz formula. A nonlinear filter with outlier rejection is applied to along-track data. We used altimeter data from Seasat, Geosat, ERS-1, ERS-2 and TOPEX/POSEDION missions. Retracked ERS-1 waveforms are shown to improve the accuracy of estimated gravity anomalies. For the three methods, the RMS differences between altimetry-derived gravity anomalies and shipborne gravity anomalies are 9.96 (differenced height) and 10.26 (height slope), 10.44 and 10.73 mgals, respectively. The RMS differences between shipborne gravity anomalies with gravity anomalies from retracked and non-retracked ERS-1 waveforms are 11.63 and 14.74 mgals, indicating retracking can improve the accuracy.

Keywords. Altimetry, gravity anomaly, collocation, inverse Vening-Meinesz, retracking

1 Introduction

Coastal gravity data from satellite altimetry have been very useful in practical applications such as coastal geoid modeling and offshore geophysical explorations, see, e.g., Hwang (1997), Andersen and Knudsen (2000). Recent global altimeter-derived gravity anomaly grids by, e.g., Sandwell and Smith (1997), Andersen et al. (2001), and Hwang et al. (2002), show that the accuracies of estimated gravity anomalies range from 3 to 14 mgals, depending on gravity roughness, data quality and areas of comparison. These papers made their comparisons with shipborne gravity anomalies mostly in the open oceans. Over shallow waters, altimeter data are prone to measurement errors and errors in geophysical corrections. For example, Deng et al. (2002) shows that within about 10 km to the coastlines, altimeter waveforms are not what the onboard tracker has expected and use of ocean mode product altimetry leads to error in range measurement. The footprint of a radiometer is also large enough to make the water vapor contents measurement near shores highly inaccurate, yielding bad wet tropospheric corrections. Large tide model errors and large wave heights, among others, add to the problem of poor quality in altimeter data over shallow waters. Worst still, there is no data on land for near-shore gravity computation and this poses a theoretical problem in transformation of functionals of the earth's gravity field (for example, transforming gravity anomaly to geoid requires global integration). Thus, gravity anomaly prediction over shallow waters has been a challenging task, due mainly to both data and theory problems.

In view of these problems, this paper compares three methods of gravity computation from altimetry, and investigate the effect of waveform retracking on accuracy of estimated gravity anomaly. A method of outlier removal in altimeter data based on a nonlinear filter is also discussed. The test area is over shallow waters near Taiwan. Fig. 1 shows the bathymetry near Taiwan based on the ETOPO5 depth grid. The waters west of Taiwan is a part of the east Asia continental shelf with depths less than 200 meters, while the waters east of Taiwan is deep due to the subducting Philippine Sea Plate.

International Association of Geodesy Symposia, Vol. 126
C Hwang, CK Shum, JC Li (eds.), International Workshop on Satellite Altimetry

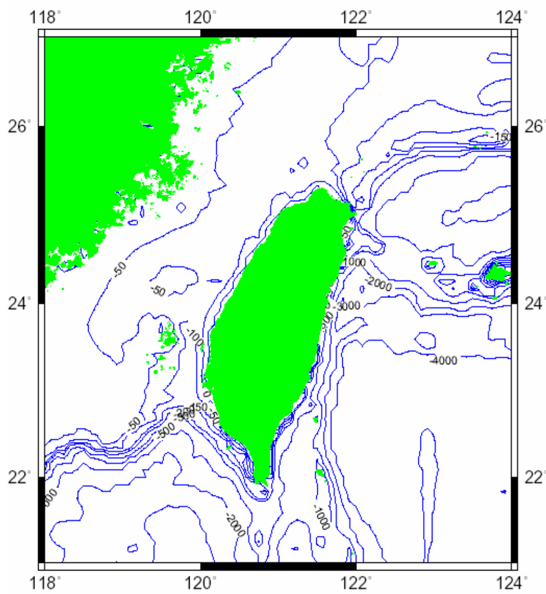

Fig. 1 Contours of slected depths around Taiwan, unit is meter

2 Three Methods of Gravity Anomaly Computations

2.1 Method of Singly Differenced Height

It has been shown by, e.g., Hwang and Parsons (1995), Sandwell and Smith (1997), that use of along-track deflection of the vertical (DOV) for derivation of gravity anomaly from altimetry can reduce the effect of long wavelength errors in altimeter data. A typical long wavelength error is orbit error. In using DOV satisfactory result can be obtained without crossover adjustment of SSH, and this is especially advantageous in the case of using multi-satellite altimeter data. Along-track DOV is defined as

$$\varepsilon = -\frac{\partial h}{\partial s} \tag{1}$$

where h is geoidal height obtained from subtracting dynamic ocean topography from sea surface height (SSH), and s is the along-track distance. The problem with (1) is that DOV can only be approximately determined because along-track geoidal heights are given on discrete points. A data type similar to along-track DOV is differenced height defined as

$$d_i = h_{i+1} - h_i \tag{2}$$

where i is index. Using differenced height has the same advantage as using along-track DOV in terms of mitigating long wavelength errors in altimeter data. To use differenced height for gravity estimation, one may employ the least-squares collocation (LSC) (Moritz, 1980). First, the covariance function between two differenced heights is

$$\begin{aligned}\operatorname{cov}(d_i, d_j) &= \operatorname{cov}(h_{i+1} - h_i, h_{j+1} - h_j) \\ &= \operatorname{cov}(h_{i+1}, h_{j+1}) - \operatorname{cov}(h_{i+1}, h_j) - \operatorname{cov}(h_i, h_{j+1}) + \operatorname{cov}(h_i, h_j)\end{aligned} \tag{3}$$

The covariance function between gravity anomaly and differenced height is

$$\begin{aligned}\operatorname{cov}(\Delta g, d_i) &= \operatorname{cov}(\Delta g, h_{i+1} - h_i) \\ &= \operatorname{cov}(\Delta g, h_{i+1}) - \operatorname{cov}(\Delta g, h_i)\end{aligned} \tag{4}$$

We go one step forwards by using "height slope" defined as

$$\chi_i = \frac{h_{i+1} - h_i}{s_i} \tag{5}$$

where s_i is the distance between points associated with h_i and h_{i+1}. The needed covariance functions are then

$$\operatorname{cov}(\chi_i, \chi_j) = \frac{1}{s_i s_j} \operatorname{cov}(d_i, d_j) \tag{6}$$

$$\operatorname{cov}(\Delta g, \chi_i) = \frac{1}{s_i} \operatorname{cov}(\Delta g, d_i) \tag{7}$$

The spectral characteristics of height slope are the same as DOV and gravity anomaly as they are all the first spatial derivatives of earth's disturbing potential. The advantage of using height slope is similar to that of using differenced height in terms of error reduction.

With differenced height or height slope, gravity anomaly can be computed using the standard LSC formula

$$\Delta g = C_{sl} (C_l + C_n)^{-1} l \tag{8}$$

where vector l contains differenced heights or height slopes, C_l and C_n are the signal and noise parts of the covariance matrices of *l,* and C_{sl} is the covariance matrix of gravity anomaly and differenced height or height slope. Differenced height or height slope can also be used for computing geoidal undulation: one simply replaces C_{sl} by the covariance matrix of geoid and differenced height or height slope in (8). Furthermore, for two consecutive differenced heights along the same satellite pass, a correlation of -0.5 exits and must be taken into account the C_n matrix in (8).

2.2 Method of Least-squares Collocation with Geoid Gradients

This method uses along-track DOV defined in (1) and the LSC method for gravity anomaly derivation (Hwang and Parsons, 1995). For this method, the covariance function between two along-track DOV is needed and is computed by

$$\begin{aligned} C_{\varepsilon\varepsilon} &= C_{ll}\cos(\alpha_{\varepsilon_p} - \alpha_{pq})\cos(\alpha_{\varepsilon_q} - \alpha_{pq}) + \\ &C_{mm}\sin(\alpha_{\varepsilon_p} - \alpha_{pq})\sin(\alpha_{\varepsilon_q} - \alpha_{pq}) \end{aligned} \tag{9}$$

where α_{ε_p} and α_{ε_q} are the azimuths of DOV at point *p* and *q*. respectively, and C_{ll} and C_{mm} are the covariance functions of longitudinal and transverse DOV components, respectively and α_{pq} is the azimuth from *p* to *q*. The covariance function between gravity anomaly and along-track DOV is computed by

$$C_{\Delta g\varepsilon} = \cos(\alpha_{\varepsilon_Q} - \alpha_{QP})C_{l\Delta g} \tag{10}$$

where $C_{l\Delta g}$ is the covariance function between longitudinal component of DOV and gravity anomaly. C_{ll}, C_{mm} and $C_{l\Delta g}$ are isotropic functions depending on spherical distance only. With these covariance functions, gravity anomaly can be computed by LSC as in (8) using along-track DOV for *l* and covariance matrices computed with $C_{\varepsilon\varepsilon}$ and $C_{\Delta g\varepsilon}$ for C_l and C_{sl}. For the detail of this method, see Hwang and Parsons (1995).

2.3 Method of Inverse Vening Meinesz Formula

This method employs the inverse Vening Meinesz formula (Hwang, 1998) to compute gravity anomaly. The inverse Vening Meinesz formula reads:

$$\begin{aligned} \Delta g_p &= \frac{\gamma_0}{4\pi}\iint_\sigma H'\left(\zeta_q \cos\alpha_{qp} + \eta_q \sin\alpha_{qp}\right)d\sigma_q \\ &= \frac{\gamma_0}{4\pi}\iint_\sigma H'\varepsilon_{qp}d\sigma_q \end{aligned} \tag{11}$$

where *p* is the point of computation, γ_0 is the normal gravity, ς_q and η_q are the north and east components of DOV, α_{qp} is the azimuth from point *q* to point *p*, and H' is the kernel function defined by

$$H' = -\frac{\cos\frac{\psi_{pq}}{2}}{2\sin\frac{\psi_{pq}}{2}} + \frac{\cos\frac{\psi_{pq}}{2}\left(3 + 2\sin\frac{\psi_{pq}}{2}\right)}{2\sin\frac{\psi_{pq}}{2}\left(1 + \sin\frac{\psi_{pq}}{2}\right)} \tag{12}$$

where ψ_{pq} is the spherical distance, see also Fig. 2. In the practical computation, the 1D FFT method is used to implement the spherical integral in (11). For the 1D FFT computation, the two DOV components ς_q and η_q are prepared on two regular grids. We use LSC to obtain ς_q and η_q on the grids along-track DOV by LSC, see also Hwang (1998).

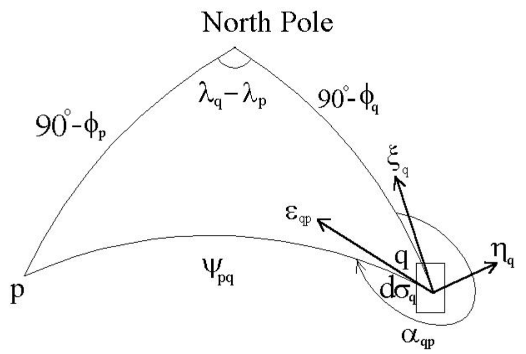

Fig. 2 Geometry for the inverse Vening-Meinesz formula

3 Use of Retracked ERS-1 Data

Zwally and Brenner (2001) and Deng et al. (2002), among others, have shown that altimeter range measurement near shores are corrupted but can be corrected by retracking the returned waveforms of altimeter. Waveform retracking uses an analytical function to fit the returned waveforms and then to determine the most appropriate epoch that should be used to calculate the travel time between the altimeter and sea surface, thereby determining the best possible rang. In general the onboard software has such a tracking capability but it is only suitable for ocean-like waveforms. Other details of waveform retracking can be found, in, e.g., Zwally (2001) and Deng et al. (2002).

In order to see whether retracked waveforms will improve gravity accuracy over shallow waters, we obtain ERS-1 waveforms from European Space Agency. The data period is from July 28, 1993 to June 2, 1996, covering ERS-1 phases C, E, F and G. The data distribution is shown in Fig. 3. This data set is also used in Anzenhofer and Shum (2001). We used the same algorithm as used in Anzenhofer and Shum (2001) to retrack ERS-1 waveforms. The waveforms are approximated by the five-parameter function

$$y_n = \beta_1 + \beta_2(1+\beta_5 Q)P(\frac{n-\beta_3}{\beta_4}), n = 1,\ldots,64 \quad (13)$$

where n is the waveform sequence, P is the error function, β_i's are parameters to be determined and Q is defined as

$$Q = \begin{cases} 0 & \text{for } n < \beta_3 + 0.5\beta_4 \\ n-(\beta_3+0.5\beta_4) & \text{for } n \ge \beta_3 + 0.5\beta_4 \end{cases} \quad (14)$$

Fig. 4 shows an example of waveforms and the approximating function and Fig. 5 shows the corrections of ranges by retracking. AS seen in Fig. 5, the corrections due to retracking are large near coastal line and small in the open oceans. Retracking also improves the estimate of significant wave height and in turn improves sea state bias.

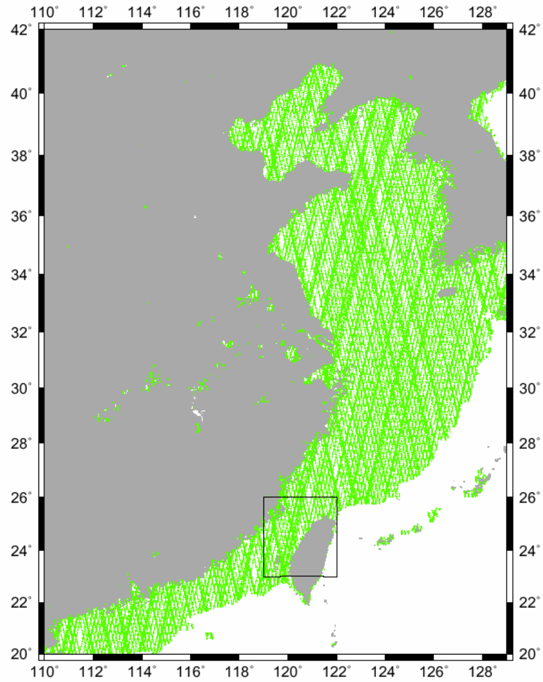

Fig. 3 Distribution of ERS-1 waveform data

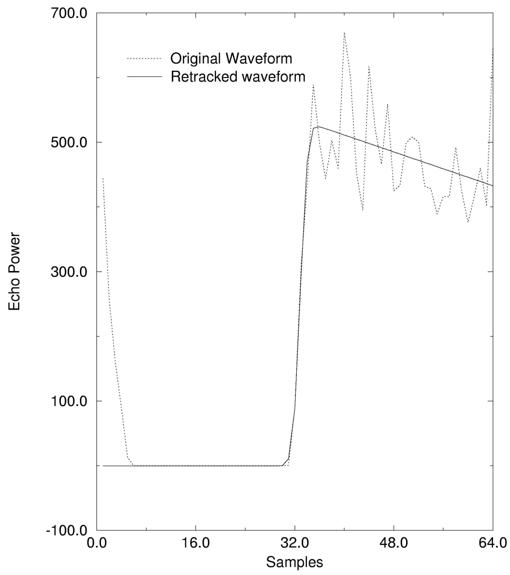

Fig. 4 Waveforms from a segment of pass 163, Cycle 11 of the ERS-1 Phase C mission and the approximating function.

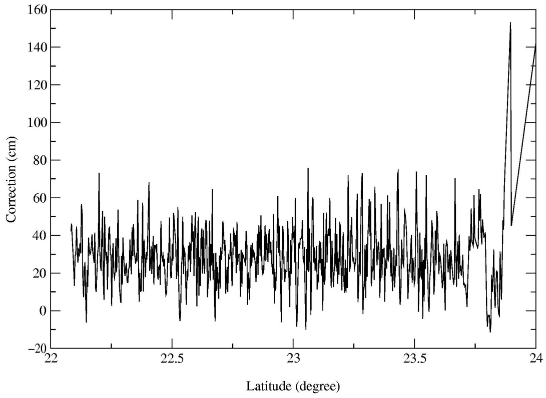

Fig. 5 Correction due to retracking along pass 163, Cycle 11 of the ERS-1 Phase C mission, as a function of latitude. Pass 163 approaches coasts at latitude near 24°N.

4 Removing Outliers

Outliers in data will create a damaging result. Methods for removing outliers in one-dimensional time series are abundant in literature, see, e.g., Kaiser (1999), Gomez et al. (1999) and Pearson (2002). In this paper we use an iterative method to remove outliers in along-track altimeter data. Consider height or differenced height as a time series with along-track distance as the independent variable. First, a filtered time series is obtained by convolving the original time series with the Gaussian function

$$f(x) = e^{-\frac{x^2}{\sigma^2}} \tag{15}$$

where σ is the 1/6 of the given window size of convolution. The definition of Gaussian function is the same as that used in GMT (Wessel and Smith, 1995). For all data points the differences between the raw and filtered values are computed, and the standard deviation of the differences is found. The largest difference that also exceeds three times of the standard deviation is considered an outlier and the corresponding data value is removed from the time series. The cleaned time series is filtered again and the new differences are examined against the new standard deviation to remove a possible outlier. This process stops when no outlier is found.

We choose pass d64 of Geosat/ERM, which travels across Taiwan, to be used for the test of outliers detection. Fig. 6 shows the ground track of pass d64 and Fig. 7 shows the result of outlier removing. In Fig.7, we clearly see that erroneous differenced heights are successfully removed (discrete points) after outlier detection with a 28-km window. For the non-repeat satellite mission such as Seasat, ERS-1/gm and Geosat/gm, we do outlier detection as well as filtering for the differenced heights with a 14-km wavelength in order to reduce the data noise. There is no need of filtering for the differenced heights from the repeat missions because their data noises will be reduced due to time averaging. As an example, we choose pass a27 of Geosat/GM for testing outlier removal and filtering. .Fig. 8 shows the ground pass a27 and Fig. 9 shows the result. Again, our algorithm removes outliers and filter the data successfully.

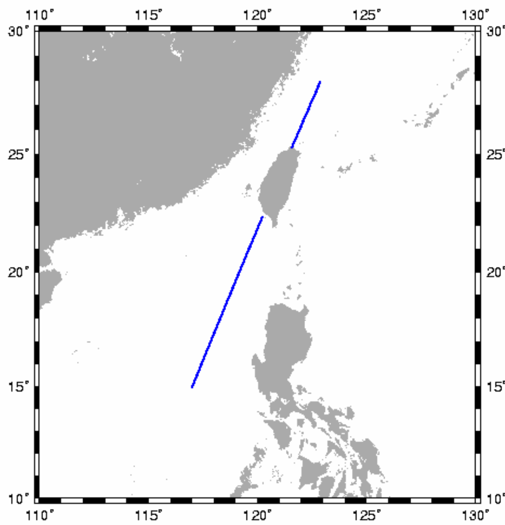

Fig. 6 The ground track of pass d64 of Geosat/ERM

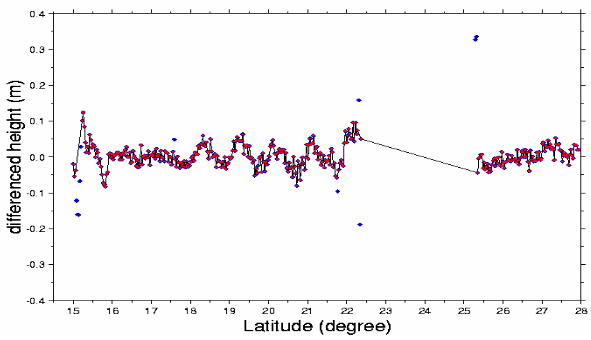

Fig. 7 Raw data points (red) and outliers (green) detected with a 28-km window for pass d64 of Geosat/ERM.

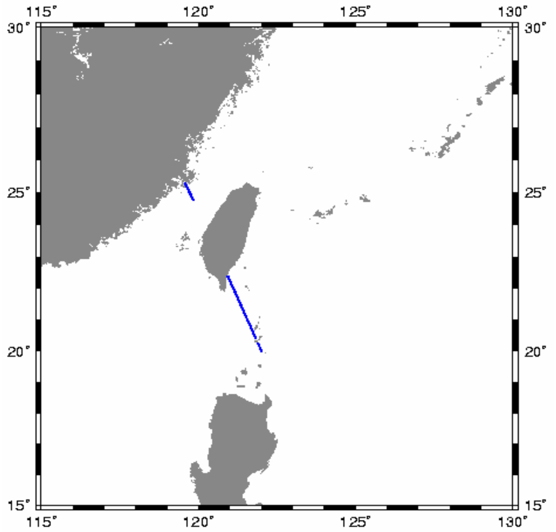

Fig 8 The ground track of pass a27 of Geosat/GM

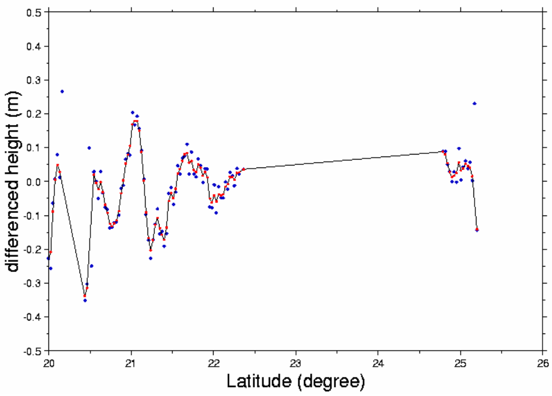

Fig 9: Raw data points (blue) and filtered and outlier-free points (red) using a 14-km window for pas a27 of Geosat/gm.

5 Altimeter Data and Results

We use altimeter data from Seasat, Geosat ERS-1/GM, ERS-1, ERS-2 and TOPEX/POSEIDON missions for testing the three methods. Table 1 summarizes the missions and data characteristics. The orbits and geophysical correction models associated with these data are the most up-to-dated. For example, the Geosat data are based on the JGM-3 orbits. Theses data have different noise levels, which work as weights in LSC computations. In all computations, the standard remove-restore procedure is employed. In this procedure, the long wavelength part of altimeter-derived data (differenced height, height slope or DOV) implied by the EMG96 geopotential model (Lemoine et al. 1998) to degree 360 is removed. With the residual data, the residual gravity anomaly is computed and finally the gravity anomaly implied by the EMG96 model is restored. The needed isotropic covariance functions are computed using the error covariance of EGM96 and the Tscherning/Rapp Model 4 signal covariance (Tscherning and Rapp, 1974). All needed covariance functions are tabulated at an interval at of 0.01°. The local covariance values in a prediction window are scaled by the ratio between the data variance and the global variance.

Table 1. Altimeter data used

Mission	Repeat Period (day)	Data duration	Cross-track sapcing (km)
Seasat	no	78/8-78/11	165
Geosat/GM	no	85/03-86/09	4
Geosat/ERM	17	86/11-90/01	165
ERS1-/35d	35	92/04-93/12 95/03-96/06	80
ERS-1/GM	no	94/04-95/03	8
ERS-2/35d	35	95/04-98/10	80
T/P	10	92/12-00/06	280

For the gravity grids from methods 1 and 2, a further filtering be 2 2-D median filter improved the result. Table 2 shows the results of such filtering. Based on the testing result for method 2 in Table 2, we decide to use 16 km as the filter parameters.

To evaluate the accuracy of the gravity anomalies derived from three different methods mentioned, we made comparisons between the predicted and shipborne anomalies in the Taiwan Strait area. These shipborne gravity anomaly data are from Hsu et al. (1998) and a pointwise comparison was made for them. The ship tracks are shown in Fig. 10. The number of ship-data used in the comparisons is 1028. Table 3 shows the result of the comparisons. The gravity grid from method 1 has a slightly better accuracy than those from the other two methods. Table 4 shows a comparison of gravity accuracies from retracked and non-retracked ERS-1 data. From Table 4 the retracked solution is better than that with non-retracked solution in the estimation.

Table 2. RMS differences (in mgals) between predicted and shipborne gravity anomalies using different filter parameters over the Taiwan Strait.

Filter parameter	RMS
No filter	11.2687
Filter wavelength = 8 km	10.8739
Filter wavelength = 16 km	10.4353
Filter wavelength = 24 km	10.5682

Table 3. Statistics of differences (in mgals) between altimeter-derived and shipborne gravity anomalies

Method	Mean	RMS	Minimum	Maximum
(1) LSC (differenced height)	8.02	9.96	-12.21	24.84
(1) LSC (height slope)	7.94	10.26	-9.39	28.96
(2)LSC (DOV)	7.70	10.44	-10.97	29.38
(3) inverse Vening Meinesz (DOV)	7.59	10.73	-14.88	29.37

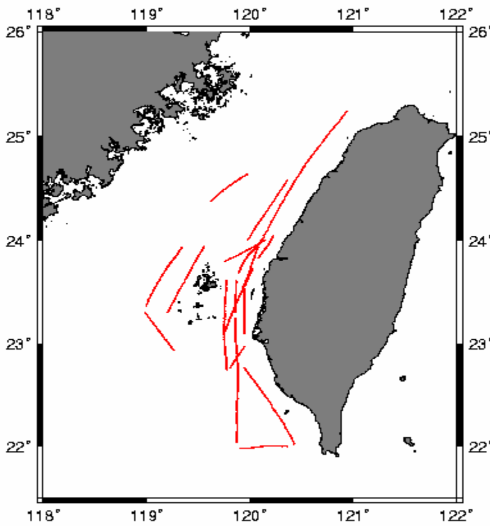

Fig. 10 Distribution of shipborne gravity data in Taiwan Strait area.

Table 4. Statistics of differences (in mgals) between altimeter-derived and shipborne gravity anomalies in case of using and not using retracked ERS-1 waveforms

	Mean	RMS	Minimum	Maximum
Before retracking	-4.86	14.74	-41.62	32.71
After retracking	-6.09	11.63	-41.08	19.82

6 Conclusions

This paper compares three methods of gravity anomaly derivation from altimetry data and use retracked ERS-1 waveforms over shallow waters. The use of differenced geoidal heights produced the best accuracy over Taiwan Strait. An iterative method to remove outliers in along-track altimeter data improves altimeter data quality and improves the accuracy of predicted gravity anomaly. Retracked ERS-1 height also improves the gravity anomaly accuracy. Use of along-track DOV with LSC yields a better result compared to the result from the inverse Vening Meinesz formula. However, the inverse Vening-Meinesz formula with 1D FFT is the fastest methods among the three. Future studies will focus on shallow waters over the Yellow Sea, East China Sea, South China Sea and Southeast Asia.

References

Andersen, O. B., and P. Kundsen (2000). The Role of Satellite Altimetry in Gravity Field Modeling in Coastal Areas, Phys Chem Earth Solid Earth Geod, 25, pp. 17-24.

Andersen, O. B., P. Kundsen and R. Trimmer (2001). The KMS2001 Global Mean Sea Surface and Gravity Field, IAG2001 Scientific Assembly, Budapest, Hungary, September.

Anzenhofer, M., C. K. Shum and M. Renstch (2001). Coastal Altimetry and Applications, Rep of Dept of Geod Sci and Surveying, in press, Ohio State University, Columbus.

Deng, A., W. Featherstone, C. Hwang and P. Berry (2002). Waveform Retracking of ERS-1, Mar Geod, in press.

Gomez, V., A. Maravall and D. Pena (1999). Missing Observations in ARIMA Models: Skipping Approach Versus Additive Outlier Approach, J Econometrics, 88, pp. 341-363.

Hsu, S., C. Liu, C. Shyu, S. Liu, J. Sibue, S. Lallemand, C. Wang and D. Reed (1998). New Gravity and Magnetic Anomaly Maps in the Taiwan-Luzon Region and Their Preliminary Interpretation, TAO, 9, pp. 509-532.

Hwang, C., and B. Parsons (1995). Gravity Anomalies Derived from Seasat, Geosat, ERS-1 and TOPEX/POSEIDON Altimeter and Ship Gravity: a Case Study Over the Reykjanes Ridge, Geophys J Int, 122, pp. 551-568.

Hwang, C. (1997). Analysis of Some Systematic Errors Affecting Altimeter-derived Sea Surface Gradient with Application to Geoid Determination Over Taiwan, J Geod, 71, pp. 113-130.

Hwang, C., H. Hsu and R. Jang (2002). Global Mean Sea Surface and Marine Gravity Anomaly from Multi-satellite Altimetry: Applications of Deflection-geoid and Inverse Vening Meinesz Formulae, J Geod, 76, pp. 407-418.

Kaiser, R. (1999). Detection and Estimation of Structural Changes and Outliers in Unobserved Components, Comput Stat, 14, pp. 533-558.

Lemoine, F. G., S. C. Kenyon, J. K. Factor, R. G. Trimmer, N. K. Pavlis, D. S. Chinn, C. M. Cox, S. M. Klosko, S. B. Luthcke, M. H. Torrence, Y. M. Wang, R. G. Williamson, E. C. Pavlis, R. H. Rapp and T. R. Olson (1998). The Development of Joint NASA GSFC and the National Imagery and Mapping Agency (NIMA) Geopotential Model EGM96, Rep NASA/TP-1998-206861, National Aeronautics and Space Administration, Greenbelt, MD.

Moritz, H. (1980). Advanced Physical Geodesy, Herbert Wichmann, Karlsruhe.

Pearson, R. K. (2002). Outliers in Process Modelling and Identification, IEEE Trans Contr Syst Tech, 10, pp. 55-63.

Sandwell, D. T., and W. H. F. Smith (1997). Marine Gravity Anomaly from Geosat and ERS-1 Satellite Altimetry, J Geophys Res, 12, pp. 10039-10054.

Tscherning, C. C., and R. H. Rapp (1974). Closed Covariance Expressions for Gravity Anomalies Geoid Undulations and Deflections of the Vertical Implied by Anomaly Degree Variance Models, Rep 208, Dept of Geod Sci, Ohio State University, Columbus.

Wessel, P., and W. H. F. Smith (1995). New Version Generic Mapping Tools Release, EOS Trans, AGU, pp. 76.

Zwally, H. J., and A. C. Brenner (2001). Ice Sheet Dynamics and Mass Balance, in LL Fu and A Cazenave (eds), Satellite altimetry and earth sciences, pp. 351-370, Academic press, New York.